HATSOPOULOS MICROFLUIDS LABORATORY
Department of Mechanical Engineering, Massachusetts Institute of Technology

Two-Dimensional Self-Assembly in Diblock Copolymers

A.E. Hosoi, Dmitriy Kogan, C.E. Devereaux,
Andrew J. Bernoff, and S.M. Baker

June 20, 2005
HML Report Number 05-P-07

HML@MIT
http://web.mit.edu/fluids

Two-Dimensional Self-Assembly in Diblock Copolymers

A. E. Hosoi,[1,*] Dmitriy Kogan,[2] C. E. Devereaux,[3] Andrew J. Bernoff,[3] and S. M. Baker[3]

[1]*Hatsopoulos Microfluids Laboratory, Massachusetts Institute of Technology, 77 Massachusetts Avenue, Cambridge, MA 02139*
[2]*California Institute of Technology, Pasadena, CA 91125*
[3]*Harvey Mudd College, 301 E. 12th Street, Claremont, CA 91711*

(Dated: June 3, 2005)

Diblock copolymers confined to a two-dimensional surface may produce uniform features of macromolecular dimensions ($\sim 10 - 100$ nm). We present a mathematical model for nanoscale pattern formation in such polymers which captures the dynamic evolution of a solution of poly(styrene)-*b*-poly(ethylene oxide), PS-*b*-PEO, in solvent at an air-water interface. The model has no fitting parameters and incorporates the effects of surface tension gradients, entanglement or vitrification, and diffusion. The resultant morphologies are quantitatively compared with experimental data.

PACS numbers: 36.20.-r, 68.18.-g, 68.55.-a, 68.03Hj

The functional flexibility and stability of polymeric films plays a crucial role in many commercial applications from protective coatings to dielectric layers in solid state electronics. While the stability properties of such films have been studied for many decades [1] a recent resurgence of interest in these systems [2–7] has arisen, driven partially by the miniaturization of technology. In order to better predict and control the self-assembled, two-dimensional structures that arise in polymeric films, we develop a new mathematical model that captures the evolution of a diblock copolymer monolayer at an air-water interface. Unlike the structures observed in three-dimensional and thin film phase segregation, the patterns in this two-dimensional system are dynamically selected and may be trapped in configurations that do not necessarily reflect thermodynamic equilibrium structures.

It is well-known that diblock copolymers with immiscible blocks are excellent materials for self-assembly of three-dimensional patterns due to the microphase separation which can produce features that are naturally nanometers in scale [8, 9]. However, confining the material to a monolayer increases the interfacial contributions due to the substrate and the environment, and changes the mechanisms responsible for such features. Here we study the spreading of a diblock copolymer, poly(styrene)-*b*-poly(ethylene oxide), PS-*b*-PEO, at an air-water interface and the two-dimensional structures that result [10–13].

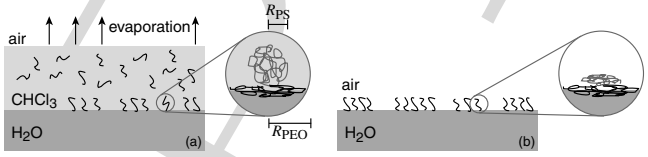

FIG. 1: (a) When the solution contacts the water, individual polymers rapidly orient with the PEO at the air-water interface (black) and the hydrophobic PS (gray) in the solvent. (b) Collapsed PS chains after the solvent has evaporated.

The proposed mechanism for this two-dimensional self-assembly differs fundamentally from both the microphase segregation that occurs in three-dimensional pattern formation, which is thermodynamic in origin and not dynamically driven [14], and from van der Waals driven spinodal decomposition, commonly associated with dewetting and rupture in ultra-thin films. In classic phase segregation, an energy cost is associated with the interface between the two types of polymers; hence the blocks associate to form equilibrium structures such as lamallae or micelles or other morphologies that minimize this interfacial cost, depending on the geometrical constraints of the system. In contrast, the final structures in the present PS-*b*-PEO system are kinetically trapped. When a droplet of polymer is deposited on the water surface via a solubilizing agent, the polymer rapidly adopts a bilamellate configuration with PEO at the air-water interface and the PS above in the air (see Figure 1). This initial three-dimensional orientation process, driven by the interface, corresponds to the classic mode of phase segregation and occurs almost instantaneously. Subsequently, the droplet spreads at the aqueous interface, simultaneously increasing the local polymer solution concentration as the solvent evaporates, and decreasing the local surface density as more area is covered.

Properties of the PS-*b*-PEO used in the experimental study [10] are listed in Table 1. Solutions of a variety of diblock copolymers in chloroform were deposited on an ultra-pure water surface in a Langmuir-Blodgett (LB) trough. The resultant monolayer films were compressed to a surface pressure corresponding to a PEO density below the phase transition to three dimensions. The film was then transferred to a silicon substrate by the LB technique. Substrates were imaged using surface force microscopy (SFM). Sample images are shown in Figure 2.

Depending on the percent of PEO in the polymer and the initial concentration of the solution, a variety of mor-

*Electronic address: peko@mit.edu

Total MW (in kDaltons)	%PEO (by mass)	MW PS (in thousands)	N_{PEO}
141.1	11	125	350
250.3	16	211.5	910
62.5	18	51	255
288	21	227	1375
38.2	22	29.8	190
89.6	34	58.6	690
80	36	51	655
129.6	55	58.6	1620
200	60	80	2725
479	90	46.5	9800
375	92	30	7840

TABLE I: Properties of pure polymers used in experiments. N_{PEO} is the number of PEO monomers.

phologies were observed including dots, stripes and larger structures known as continents. The predominant features that result exhibit characteristic length scales on the order of tens of nanometers and can be controlled by a judicious choice of relative block size and spreading solution concentration [11]. All features have a vertical thickness of one molecule ($\sim$ 5nm). For the molecular weights and relative volume fractions listed in Table 1, dots have diameters on the order of 70-80nm and tend to be arranged in regular hexagonal lattices.

The observed morphologies of the polymers can be controlled experimentally by varying %PEO and solution concentration. At a weight fraction of 7% PEO, the projected area of the two dimensional PEO pancake at the interface is approximately equal to the projected area of the PS (see Figure 1). PS, a three-dimensional hydrophobic "blob," avoids the aqueous interface and will aggregate with neighboring PS, in the presence of solvent, if the blocks are sufficiently close [15]. Below 7%, the probability of PS overlap is great and the PS/PS attraction tends to overwhelm the PEO/PEO repulsion. Hence continents tend to form at 7% or below. Conversely, above 15% the repulsion between PEO pancakes supersedes the PS/PS attraction; aggregation is reduced and dots are the predominant feature. Between 8–13% PEO, when the projected areas of the PS and PEO are roughly equal, a mixture of stripes and dots are observed. Solution concentration sets the initial condition for the droplet on the surface and limits the amount of separation or spreading that occurs before the solvent has fully evaporated. Increasing the initial concentration shifts the predominant feature from dots to stripes to continents.

To model the evolution leading to these structures, we incorporate four primary effects: Marangoni forces, evaporation of solvent, entanglement or vitrification of long polymer chains, and diffusion of the polymers along the air-water interface. Poly(ethylene oxide), PEO, is a surfactant that remains localized at the surface in a two-dimensional "pancake" provided the surface density does not exceed $\sim$ 1 PEO monomer/20 $\mathring{A}^2$ (see Figure 1). Forces resulting from gradients in surface tension (Marangoni), due to variations in PEO concentration, are proportional to the local concentration gradient, $\mathbf{F}_{\mathrm{ST}} = \sigma(c)\nabla c$, where the coefficient, $\sigma(c)$, is measured experimentally [11]. The function $c(x, y, t)$ describes the local polymer concentration field where "concentration" refers to the two-dimensional density of polymers at the interface i.e. $c(x, y, t) = (\text{mean molecular area})^{-1}$. Surface tension as a function of concentration, $\gamma(c)$, was approximated, as $\gamma_{\mathrm{H_2O}} - \gamma(c) = 5(1-\tanh[1/(cR^2_{\mathrm{PEO}})-4])\mathrm{mN/m}$, by fitting data from [10]. Integrating this function around the perimeter of a PEO pancake and Taylor expanding about a uniform initial concentration, c_0, we find the Marangoni force acting on a single polymer [21]:

$$\mathbf{F}_{\mathrm{ST}} = \pi R^2_{\mathrm{PEO}} \left.\frac{\partial \gamma}{\partial c}\right|_{c_0} \nabla c \equiv \sigma(c)\nabla c. \tag{1}$$

As the polymers spread, solvent continues to evaporate and the PS chains associate and begin to vitrify. This entanglement/vitrification force between two polymers is modeled as a non-Hookean elastic network [16], with the force between two polymers given by $f_{\mathrm{E}} = 3kT(1/r - r/r_0^2)$ [22] where T is temperature, k is Boltzmann's constant, l is length of one monomer, N is the number of PS monomers and $r_0^2 = Nl^2$ Two polymers are considered "entangled" if the PS blobs overlap. Note that entanglement is indistinguishable from vitrification in this physical picture and the detailed mechanism for the connection between two polymers is irrelevant.

The radii of the PS blobs are constantly fluctuating due to thermal effects thus the probability that a PS blob has an instantaneous radius, r_i, is given by $P(r_i) = 4\pi r_i^2 (3/2\pi N l^2)^{3/2} e^{-(3r_i^2/2Nl^2)}$. The expected value of the force between two polymers may then be written as $f(r) = \iint \tilde{f}(r) P(r_1) P(r_2)\, dr_1 dr_2$ where $\tilde{f}(r) = f_{\mathrm{E}}(r_1) + f_{\mathrm{E}}(r_2)$ if the polymers overlap and zero otherwise. Here r is the separation between the centers of the two interacting polymers, and r_1 and r_2 are the instantaneous radii of the PS blobs. This expected force value, $f(r)$, (shown in Figure 3a for an interaction between two 51k polymers) is integrated over all pairwise interactions to obtain the effective spring force at a point $\mathbf{r}_0$. The concentration field is then Taylor expanded about $\mathbf{r}_0$ and only the two lowest order non-zero contributions are retained yielding the force due to vitrification or entanglement between two polymers:

$$\mathbf{F}_{\mathrm{E}}(\mathbf{r}_0) = \pi \left(\alpha_2 \nabla c + \frac{\alpha_4}{8} \nabla \nabla^2 c \right) \tag{2}$$

where α_n is defined as the nth moment of the pairwise force function, $\alpha_n \equiv \int_0^\infty r^n f(r)\, dr$. Note that we expect this approximation to be valid provided the concentration field varies over a characteristic length scale that is long compared to the typical length scales associated with $f(r)$.

As the Reynolds number is very small ($< 10^{-5}$), the system is overdamped and we neglect inertia of both polymer and fluid phases. In such a system, any velocity

is a direct consequence of the instantaneous forces and we model an individual polymer as a sphere of radius $R_{\rm PS}$ moving through chloroform:

$$\mathbf{v} = \frac{\mathbf{F}_{\rm ST}(c) + \mathbf{F}_{\rm E}(c)}{6\pi R_{\rm PS}\mu} \tag{3}$$

where μ is the viscosity of the chloroform and $R_{\rm PS}$ is the radius of gyration of the PS.

Finally, this velocity in inserted into a two dimensional transport equation for polymer concentration. Evaporation decreases the mobility of the polymers and can be included by multiplying the velocities by a phenomenological mobility envelope that decreases monotonically with time (e.g. $e^{-\beta t}$). Again, as with the entanglement force function, the resulting morphologies and length scales are not sensitive to the precise form of the mobility envelope. The final component of the model is to introduce a cutoff function, $f_{\rm c} = [1 - \tanh(c - c_{\rm max})]/2$, that reflects the fact that the PEO is incompressible i.e. the maximum allowable surface concentration is set by the area of the PEO pancakes. Changing variables by defining $\tau = (1 - e^{-\beta t})/(6\pi\beta R_{\rm PS}\mu)$ yields our final evolution equation:

$$\frac{\partial c}{\partial \tau} = \nabla \cdot \left[f_{\rm c} \left(c \left[(\sigma - \pi\alpha_2)\nabla c - \frac{\pi}{8}\alpha_4 c \nabla\nabla^2 c \right] + kT\nabla c \right) \right] \tag{4}$$

where the diffusivity of the polymers along the air-water interface has been approximated as the Einstein diffusivity, $kT/(6\pi\mu R_{\rm PS})$.

Equation (4) may be reduced to a standard Cahn-Hilliard [17, 18] form,

$$\frac{\partial c}{\partial \tau} = \nabla \cdot \left[M(c) \nabla \left(\frac{\partial q}{\partial c} - K\nabla^2 c \right) \right] \tag{5}$$

by defining $M(c) = c f_{\rm c}$, $K = \frac{\pi}{8}\alpha_4$ and $q = \frac{(\sigma - \pi\alpha_2)}{2}c^2 + kT(\ln c - 1)$. It is well-known that equation (5) can lead to spinodal decomposition, i.e. uniformly mixed states may be metastable and evolve into phase segregated domains. However, it is important to note that the Cahn-Hilliard equation is often treated as a phenomenological model used to generically mimic phase separation whereas the coefficients in equation (4) have been completely determined by ensemble averaging over microscopic physical states. Thus all coeffcients are fixed by well-defined physical parameters, and the observed characteristic length scales may be predicted from known quantities.

Typical numerical results obtained by evolving the full nonlinear equation (4) are shown in Figure 2. Parameters used in the simulations are summarized in Table 1. The numerics capture both the dot and the stripe morphologies and the transitions between the two (i.e. pearling). At the moderate concentrations used in the theoretical treatment, the features evolve quickly to dilute stripes and if possible, transition into denser dots as observed in the experiment. There are two control parameters that determine whether the stripe-to-dot transition is allowed

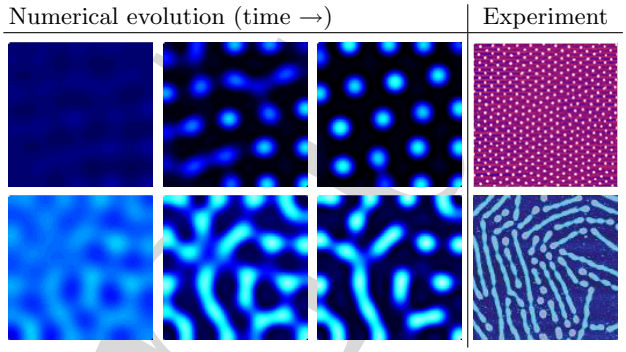

FIG. 2: Two numerical time series with different initial concentrations showing the evolution of dots and pearling compared with experimental (SFM) images. Dot diameters and stripe widths in the experimental images are both approximately 100nm. Parameters in the numerical simulation correspond to a 51k polymer with initial concentration $c_0 = 0.84 \times 10^{10}$ molecules/cm^2 (top row) and $c_0 = 3.3 \times 10^{10}$ molecules/cm^2 (bottom row). Black in the numerical data indicates a clean interface with no polymer, light colors indicate high polymer concentrations. Both PS and PEO are concentrated within the dots and stripes.

for a fixed %PEO: the cutoff function, defined by the maximum surface density allowed by the presence of the incompressible PEO, and the initial bulk concentration of polymer in solvent. In the absence of a cutoff function, the polymers can always collapse into dots spaced in a regular hexagonal lattice as there is no limit to the packing density, i.e. stripes can freely coalesce into energetically favorable dots. However, we expect the polymers to become locked in the stripe morphologies when the maximum concentration attained within the stripes approaches the maximum allowed concentration. This indicates that stripes will be observed if the initial bulk concentration of polymer in solvent is sufficiently high, consistent with experimental observations. In addition, polymers are mobile only in the presence of solvent. If there is insufficient solvent at the onset of the experiment, all of the chloroform rapidly evaporates, freezing the polymer in the stripe morphology before the transition to dots is complete. In intermediate regimes, in which the stripes begin to break into dots but are arrested by the cutoff, thin connections remain between dots and pearling is observed as shown in Figure 2.

Finally, we consider the linear stability of (4). Characteristic dot diameters, determined by the fastest growing mode, are given by

$$\lambda_{\rm crit} = \frac{2\pi}{|\mathbf{k}|_{\rm crit}} = \pi \left(\frac{\pi\alpha_4}{\pi\alpha_2 - \sigma(c_0) - kT/c_0} \right)^{1/2}. \tag{6}$$

This wavelength can be converted into an aggregate number, $AN = \pi(\lambda_{\rm crit}/2)^2 c_0$, the expected number of polymers/dot. Experimental data and linear stability predictions are summarized in Figure 3(b). Parameters used in

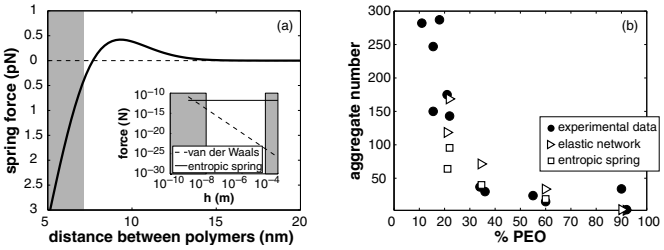

FIG. 3: (a) Expected value for the network force function and an order-of-magnitude comparison with van der Waals forces (inset). The grey shaded region in the spring force function indicates forbidden separation distances due to the incompressibility of the PEO pancake (R_{PEO} is approximately 7nm for this polymer). Grey regions in the inset indicate film thicknesses that are outside of the normal range sampled by the polymer film as the solvent evaporates during the course of the experiment. (b) Comparison of model predictions for aggregate number with experimental data. Triangles and squares indicate two different network force functions: triangles correspond to the function given in the text and squares correspond to a logarithmic entropic spring function [19]. The two experimental parameters that play a role in determining the aggregate number are %PEO and N; each data point corresponds to a particular (%PEO,N) pair as summarized in Table I.

the stability analysis are all known (summarized in Table 1) with the exception of c_0, the initial surface density, which was estimated as $c_0 \approx 0.4/N_{\mathrm{PEO}}$ molecules/$\mathring{A}^2$, consistent with experimental observations. Unlike many phenomenological models that produce dot and stripe morphologies, the present study is quantitative in the sense that dot size and aggregation number are completely predicted by microscopic properties of the polymer such as number and length of the monomers and by average properties of the system such as temperature and average initial concentration. In particular, as illustrated in figure 3(b), the most influential parameter in determining the aggregate number is the ratio of PS to PEO and by varying the %PEO, one can continuously tune the size of the observed structures [23].

While there are many other physical mechanisms that may lead to phase separation, the most common do not produce our experimentally observed scalings. For example, spinodal decomposition driven by van der Waals effects could produce similar patterns with similar length scales. However, van der Waals forces are several orders of magnitude smaller than entanglement/vitrification effects for all thicknesses sampled by the film during evaporation (see inset in Figure 3a) and the wavelengths of van der Waals driven structures scale as h^2 [3] which does not reflect the dependence on %PEO that is observed experimentally (Figure 3b).

The ability to control patterned structures by self-assembly on the molecular scale by noncovalent forces can serve as a powerful tool in developing nanoscale technologies. We have developed a system in which the behavior of diblock copolymers in two dimensions can be optimized to produce regular, uniform features of macromolecular dimensions ($\sim 10-100$ nm) and derived a new dynamic model that quantitatively captures the experimentally observed length scales and diversity of features. It is hoped that this new understanding will eventually lead to insights into mechanisms that could provide more detailed control of the observed structures using macroscopic manipulations (such as shear in the underlying fluid layer) to control microscopic properties.

Acknowledgments

The authors gratefully acknowledge Gareth McKinley, and Tom Russell for their valuable suggestions. This study was partially funded by NSF awards CCF-0323672, DMS 0243591 (AEH) and DMR-0109077, CHE-0097262 (SMB).

[1] A. Vrij, Discuss. Faraday Soc. **42** (1966).
[2] F. Brochard-Wyart and J. Daillant, Can. J. Phys. **68** (1990).
[3] F. Brochard-Wyart, P. Martin, and C. Redon, Langmuir **9**, 3682 (1993).
[4] K. Jacobs, S. Herminghaus, and K. Mecke, Langmuir **14**, 965 (1998).
[5] G. Reiter, Phys. Rev. Lett. **68**, 75 (1992).
[6] R. Xie, A. Karim, J. F. Douglas, C. C. Han, and R. A. Weiss, Phys. Rev. Lett. **81**, 1251 (1998).
[7] T. Kerle, R. Yerushalmi-Rozen, J. Klein, and L. J. Fetters, Europhys. Lett. **44**, 484 (1998).
[8] I. W. Hamley, *The Physics of Diblock Copolymers* (Oxford, New York, 1998).
[9] F. S. Bates and G. H. Fredrickson, Physics Today **52**, 32 (1999).
[10] C. A. Devereaux and S. M. Baker, Marcomolecules **35**, 1921 (2002).
[11] S. M. Baker, K. A. Leach, C. E. Devereaux, and D. E. Gragson, Macromolecules **33**, 5432 (2000).
[12] J. K. Cox, K. Yu, B. Constantine, A. Eisenberg, and R. B. Lennox, Langmuir **15**, 7714 (1999).
[13] J. Zhu, A. Eisenberg, and R. B. Lennox, Macromolecules **25**, 6547 (1992), and page 6556.
[14] E. L. Thomas, Science **286**, 1307 (1999).
[15] A. M. G. da Silva, E. J. M. Filipe, J. M. R. dOliveira, and J. M. G. Martinho, Langmuir **12**, 6547 (1996).
[16] P. J. Flory, *Principles of Polymer Chemistry* (Cornell University Press, Ithaca and London, 1953).
[17] J. W. Cahn and J. E. Hilliard, J. Chem. Phys. **28** (1958).
[18] D. Zwillinger, *Handbook of Differential Equations* (Academic Press, Boston, MA, 1997), 3rd ed.
[19] P. Atkins, *Physical Chemistry* (Freeman, 1999), 6th ed.
[20] J. Israelachvili, *Intermolecular & Surface Forces* (Academic Press, London, 1992), 2nd ed.
[21] Although it is not at all obvious that a continuum con-

cept of surface energy can be extended down to molecular scales, experimental evidence in conjunction with simple scaling arguments presented in [20] indicate that this picture remains valid even for an isolated molecule.

[22] The observed patterns and length scales are not sensitive to the exact form of the entanglement/vitrification force function and variations such as non-Hookean entropic springs [19] have also been tested. All of these models yield quantitatively similar results provided the force function scales linearly with kT.

[23] Note that the average spacing between the dots can be controlled independently by the pressure at which the film is deposited. Higher pressures correspond to lower mean molecular areas and higher packing densities.